Pergamon

PII: S0306-4522(01)00174-9

Neuroscience Vol. 105, No. 1, pp. 19–31, 2001

0306-4522/01 $20.00+0.00

www.elsevier.com/locate/neuroscience

HIGH-RESOLUTION TWO-DIMENSIONAL SPATIAL MAPPING OF CAT STRIATE CORTEX USING A 100-MICROELECTRODE ARRAY

D. J. WARREN,[a] E. FERNANDEZ[b] and R. A. NORMANN[a]*

[a]Center for Neural Interfaces, Department of Bioengineering, University of Utah, 20 South 2030 East, Rm 506, Salt Lake City, UT 84112-9458, USA

[b]Institute of Bioengineering, Universidad Miguel Hernandez, Elche, Spain

Abstract—Much of our understanding of the visuotopic organization of striate cortex results from single-electrode penetrations and serial recording of receptive field properties. However, the quality of these maps is limited by imprecision in quantifying electrode position, combining data from multiple laminae, and eye drift during the measurement of the receptive field properties. We have addressed these concerns by using an array of 100 closely spaced microelectrodes to investigate the two-dimensional visuotopic organization of layer IV in cat striate cortex. This array allowed simultaneous measurement of the receptive field properties of multiple single units on a regularly spaced grid. We found the relationship between cortical and visual space to be locally non-conformal: the receptive field locations associated with a closely spaced line of electrodes appeared randomly scattered in visual space. To quantify the scatter, we fitted a linear transformation of electrode sites onto the associated receptive field locations. We found that the distribution of the difference between the predicted receptive field location and the measured location had standard deviations of 0.59° and 0.45° in the horizontal and the vertical axes, respectively. Although individual receptive field positions differed from the predicted locations in a non-conformal sense, the trend across multiple receptive fields followed the maps described elsewhere. We found, on average, that the 13 mm^2 of cortex sampled by the array mapped onto a 5.8-$degrees^2$ region of visual space. From the scaling of this map and a combination of the statistics of the receptive field size (2.7 ± 1.5 $degrees^2$) and scatter, we have explored the impact of electrode spacing on the completeness and redundancy in coverage of visual space sampled by an array. The simulation indicated an array with 1.2-mm spacing would completely sample the region of visual space addressed by the array.

These results have implications for neuroprosthetic applications. Assuming phosphene organization resembles the visuotopic organization, remapping of visual space may be necessary to accommodate the scatter in phosphene locations.

Key words: visuotopy, receptive field, neuroprosthesis, vision prosthesis, cat visual cortex, electrode arrays.

Many researchers have studied the visuotopic organization of mammalian striate cortex. They have shown that, while cortical magnification varies with retinal eccentricity, the global visuotopic map is generally conformal (Hubel and Wiesel, 1974; Albus, 1975b; Tusa et al., 1978; Tootell et al., 1982; Dow et al., 1985; DeAngelis et al., 1999; Hetherington and Swindale, 1999). That is, nearby points in visual space are mapped onto nearby regions in striate cortex. However, when researchers focused on the local visuotopic organization of striate cortex, the receptive field characteristics of the neurons manifested properties that were inconsistent with a conformal organization. The properties of receptive fields, recorded along a single cortical column with a microelectrode track orthogonal to the cortical surface, have considerable variability both in their location in visual space and in their size. In fact, two neurons recorded simultaneously from a single microelectrode can have receptive fields that show no spatial overlap (Hubel and Wiesel, 1974). These receptive field properties argue against a simple, conformal local visuotopic organization.

The conclusions resulting from local visuotopic mapping experiments have been confounded by imprecise knowledge of the relative positions of the microelectrode recording locations (Dow et al., 1985) and by methodological problems associated with eye drift (Rodieck et al., 1967; Cicerone and Green, 1977). Typically, these studies were done using sequential recordings of receptive field properties from neurons encountered along tracks made tangential to the cortical surface. Consequently, comparisons could be made only of properties measured within a single track and then, in order to provide an adequate sample size, across multiple laminae with the commensurate changes in the degree of scatter. Further, making maps with large numbers of receptive fields required extended experimentation time, thereby introducing more opportunity for eye drift to contaminate the conclusions of the study. While the use of paralytic agents and eye immobilization can significantly reduce the extent of the eye drift, these techniques do not eliminate

*Corresponding author. Tel.: +1-801-581-7645; fax: +1-801-581-8966.

E-mail address: normann@m.cc.utah.edu (R. A. Normann).

Abbreviations: ANOVA, analysis of variance; SNR, signal to noise ratio; UEA, Utah electrode array.

the problem (Rodieck et al., 1967; Cicerone and Green, 1977).

We have investigated the local visuotopic mapping of cat striate cortex using an array of 100 penetrating microelectrodes to record simultaneously the receptive field properties of many neurons. Simultaneous recording of receptive field properties, coupled with the use of paralytic agents, greatly reduces the problems of eye drift. The fixed geometric arrangement of the electrodes reduces the uncertainties of electrode position, and the fixed length of the electrodes allows concurrent measurement of receptive field properties for a large number of neurons within a cortical lamina.

We conclude that the local visuotopic organization of striate cortex is non-conformal. In particular, given knowledge of the receptive field location recorded on one electrode, we could only poorly predict the location of the receptive field on a neighboring electrode. To have a high probability of recording non-overlapping receptive fields, we estimated electrodes would have to be separated by more than 2.0 mm. This study has implications for the design of a cortically based vision neuroprosthesis, one motivation for the development of the array utilized in this study. The organization of a field of phosphenes, evoked by electrical stimulation via our array of penetrating electrodes and having 0.4-mm interelectrode spacing, is expected to be non-conformal. Consequently, we conclude that electronic circuitry likely will have to be provided in a vision neuroprosthesis to transform visual information into a useful conformal phosphene map.

EXPERIMENTAL PROCEDURES

Experiments were performed under animal care and experimental guidelines that conformed to those set by the National Institute of Health. The experiments were designed under the goal of reduction, refinement, and replacement to minimize the pain and suffering associated with live animal experiments.

Surgical procedures

Only a brief description of the animal preparation, maintenance, and surgery procedures is given here, as they have been fully described elsewhere (Nordhausen et al., 1996). Four adult cats were used. All animals were obtained from the University of Utah Animal Resource Center. Each animal was induced with either ketamine (5–20 mg/kg, i.m.) or a cocktail of equal proportions by weight of tiletamine and zolezepam (Telazol®, Fort Dodge, Overland Park, KS, USA; 6–13 mg/kg, i.m.), cannulated, intubated, and its head immobilized. The animal was artificially ventilated and anesthesia maintained with halothane (1.0–1.5% during the surgery, 0.7–1.1% during recording). Heart rate, electrocardiogram, expired carbon dioxide, and core temperature were monitored, the latter was maintained between 37 and 40°C with a water blanket. The visual cortex was exposed by a 1–2-cm-diameter craniotomy and the dura reflected. After establishing a baseline level of anesthesia for at least 2 h, paralysis was established with pancuronium bromide (0.1 mg/kg/h, i.v.) either by an hourly bolus or by continuous infusion. The pupils were dilated with atropine sulfate (1% solution) and the nictitating membranes retracted with phenylephrine hydrochloride (neosynephrine, 10% solution). The eyelids were sutured open and gas-permeable contact lenses (0 diopters) were placed in each eye to protect the corneas. The retinas were back refracted onto a tangent screen and the focus adjusted with external lenses. The locations of retinal landmarks were recorded on the screen to assist estimation of the location of area centralis (Bishop et al., 1962; Nikara et al., 1968).

An acute configuration of the Utah electrode array (UEA, Bionic Technologies, Inc., Salt Lake City, UT, USA) was used for all experiments. The fabrication and characteristics (Jones et al., 1992) as well as the pneumatic insertion technique (Rousche and Normann, 1992) of the UEA are described elsewhere. In the acute configuration, the 1.0- or 1.5-mm-long electrodes are arranged in a 10×10 grid with 0.4-mm spacing between adjacent electrodes. The electrode impedance ranged between 100 and 600 kΩ with typical impedances around 300 kΩ, measured with a 1-kHz, 100-nA, sinusoidal signal. The UEA was implanted to a depth of 1.0 or 1.5 mm at the junction of the lateral and posterior lateral gyri, for 1.0- and 1.5-mm electrode lengths, respectively.

Electrophysiological recording

Neural activity as well as the state of the visual stimulus was recorded by a 100-channel data acquisition system (Bionic Technologies Inc.). This system amplified ($5000\times$), filtered (250–7500 Hz), and digitized the neural signals (8 bits, selectable resolution of 0.5–8 μV per bit, 30 000 samples per second). Further details of the data acquisition system are available elsewhere (Guillory and Normann, 1999). We collected data from both eyes in two of the cats. In the other two cats, we only collected data for the eye contralateral to the implant site as too few of the electrodes exhibited a response to visual stimulation of the ipsilateral eye. Neural activity was observed at 185 electrode sites out of the possible 375 sites (reduced from a potential of 400 sites due to broken electrodes and wires).

Visual stimulus

We mapped the approximate location and orientation preference of the multi-unit neural response for each electrode using bars projected onto a tangent screen with a hand-held projector. Although we noted the preferred orientation, these data are not reported here, as the measurement was qualitative. A computer monitor was placed at the approximate visual space representation of the majority of the receptive fields and a random checkerboard pattern was displayed. Initially, we used a 15-inch monitor (Viewsonic Model 15GS), placed 90 cm from the eye. In the later experiments, we used a 17-inch monitor (Hitachi Model 620), placed 80 cm from the eye. Both monitors had a 640×480 pixel resolution and 100-Hz refresh rate. The checkerboard pattern consisted of a number of equal-sized squares, each of which subtended $1.1\times1.1°$ ($1.0\times1.0°$ on the 15-inch monitor). Each square was randomly set to either black or white with a 25% probability of being white. The logical origin of the screen was selected randomly. This allowed the entire checkerboard to be shifted both vertically and horizontally by 0.14° steps (0.26° steps on the 15-inch monitor). A new checkerboard with a new logical screen offset was displayed at a rate of 25 Hz. For each measurement of the receptive field properties, visual stimuli were presented and neural data recorded for 30 min. Typically, five measurements of the receptive field characteristics were performed, lasting a total of 5 h if only the contralateral eye was examined and 10 h if both the contralateral and ipsilateral eyes were examined. Visual stimulation was presented monocularly.

Unit classification

We performed unit classification by an unsupervised statistical classification method called mixture modeling (Sahani et al., 1997; Lewicki, 1998; Jain et al., 2000). After unit classification, we reduced the set of potential units through an examination of the signal to noise ratio (SNR) and the relative timing of neural events. We removed units from the analysis if their SNR was less than two; the largest SNR observed was seven. The SNR

was defined as the ratio of the range of the amplitude of the template generated by the classification scheme to the range of the noise signal. The latter is the difference between the 95th and 5th percentiles of all data points in the first 0.33 ms of the recorded waveforms. Additionally, if multiple units on an electrode showed significant cross correlation, we removed all but one of the units from the analysis. A significant cross correlation likely had one of two sources, either the units were distinct but exhibited correlated firing or the unit classification method incorrectly separated a single unit into two or more units. We chose the more conservative interpretation, assuming the classification was in error, and removed all but the most active unit.

Data analysis

The reverse correlation method was used to estimate the receptive field properties (Jones and Palmer, 1987; Eckhorn et al., 1993). This was done by cross correlating spike times with the visual stimulus over a range of latencies between the stimulus and the spike. For the latency Δt seconds, the cross correlation resulted in a two-dimensional array of sums. Each sum enumerated the number of times the particular location of the screen was illuminated Δt seconds prior to the occurrence of a spike. The sums were examined under the null hypothesis that the stimulus and the spike were not correlated. Under this hypothesis, each sum would be binomially distributed, being the result of N independent Bernoulli trials where N is the number of spikes. As N became large, the sum could be approximated with a normal distribution having mean $N/4$ and variance $3N/16$. By subtracting out the mean and dividing by the standard deviation, the resulting statistic was distributed as a standardized normal random variable and had units of standard deviations. From the number of standard deviations observed, the probability of seeing the sum could be calculated under the assumption that the null hypothesis was valid. A large, positive value indicated that the location on the screen was illuminated more often than could be explained by chance and, hence, represented an excitatory region of the receptive field. To distinguish receptive fields from chance large sums, an acceptance criterion of 4.3 standard deviations was used. This value was selected as it implies that on average only one of the 115 200 sums from six latencies would exceed this limit when the null hypothesis was true. If the excitatory region was smaller than 0.15 degrees^2 or seen for less than 25 ms, it was considered a chance large sum and was removed from the analysis. Further, we excluded units that did not reliably generate a receptive field across repeated measurements of the properties. A reliable unit was defined as one that produced a receptive field in three of the five measurements of the properties (three animals) or in three of the four measurements (one animal).

We found 92 single units that had a reliable excitatory receptive field. Of these units, 54 were driven exclusively by visual stimulation of the contralateral eye, 17 units were driven exclusively by the ipsilateral eye, and 23 units were binocularly driven. After accepting a region as being an excitatory receptive field, we parameterized the receptive field by its peak value, latency to the peak value, size, and location. The size of the receptive field was defined as the area of the contiguous region surrounding the peak value and having magnitude greater than or equal to 4.3 standard deviations. The two-dimensional location of the receptive field was defined as the center of mass of the same region. Both the size and location were calculated at the latency of the peak value.

Fitting receptive fields

To analyze the visuotopic organization of primary visual cortex, we compared the measured receptive field positions to that estimated by a linear coordinate transformation (or a linear map) of the electrode array onto its visual space representation. The coordinate transformation allowed for five degrees of freedom: the magnification along both sides of the UEA (SF_x and SF_y), the rotation of the UEA (θ), and the translation in both the horizontal and vertical axes (OFF_a and OFF_e). A non-linear, least-mean-squared minimization method (FMINS function in MATLAB®) was used to minimize the difference between the coordinate transform and measured receptive fields. The electrode position (E_x and E_y) was related to the visual space position (V_a and V_e) by the equation

$$\begin{bmatrix} V_a \\ V_e \end{bmatrix} = \begin{bmatrix} SF_x \cos\theta & SF_y \sin\theta \\ -SF_x \sin\theta & SF_y \cos\theta \end{bmatrix} \begin{bmatrix} E_x \\ E_y \end{bmatrix} + \begin{bmatrix} OFF_a \\ OFF_e \end{bmatrix} \quad (1)$$

We interpreted our results in terms of linear mapping and conformal mapping. A conformal map is one that preserved angles. For example, the transformation on a grid printed on a rubber diaphragm that has been stretched is a conformal operation.

Statistical methods of data analysis

The Windows-based SPSS® statistics package (Release 9.0.0) was used to perform all statistical analyses. A significance level of 0.025 was used. A multi-way analysis of variance (ANOVA) with repeated measures, through the General Linear Model function, was used to compare receptive field sizes within and between animals. The distributions of the length of the residues of the fit described above were compared to the estimated measurement error by a two-sample Kolmogorov–Smirnov test. A multi-way ANOVA with repeated measures was used to compare the length of the residues and the magnification factor within and between animals. The variances of the residues in each of the horizontal and vertical axes were compared with a two-tailed variance ratio test and Kendall's τ. Each of the residues was compared to a normal distribution by a single-sample Kolmogorov–Smirnov test. The estimated measurement errors of the peak value, area, and location of the receptive field were tested for zero mean through a two-tailed t-test and normality through a single-sample Kolmogorov–Smirnov test. The variances of the location measurement error in each of the horizontal and vertical axes were compared by a two-tailed variance ratio test and Kendall's τ. Their distributions were compared through a two-sample Kolmogorov–Smirnov test. The effect of eye drift on the error in area measurement was tested through a multi-way ANOVA with repeated measures.

Histology

As the UEA did not conform to the curvature of the surface of cortex, it was expected that not all electrodes would be in layer IV when the array was inserted. To verify that the majority of electrodes were in the desired lamina, we excised the region of cortex implanted in one of the animals. At the end of the experiment, the array was explanted and the animal perfused with a solution of 4% paraformaldehyde in 0.1 M phosphate buffer (pH 7.45) by cardiac puncture. The brain was prepared for sectioning by being washed in 0.1 M phosphate buffer for 2 h and cryoprotected in 15% sucrose for 30 min, in 20% sucrose for 1 h and in 30% sucrose for 24 h at 4°C before embedding in tissue freezing medium. The brain was serially sectioned in the coronal plane into 20-μm sections on a cryostat and the sections were stained using standard Nissl procedures. The depth and location of the electrode tips for each electrode were estimated using the electrode track as a guide under a light microscope. One fortunate section showing a number of electrode tracks is shown in Fig. 1A. The tracks appear as the dark, radially oriented lines in this figure, the result of infusion of blood into the tracks. As we have never observed blood in electrode tracks of animals that were perfused with the electrodes *in situ*, we believed the blood entered the electrode tracks between array explantation and animal fixation. All of the electrode tips illustrated in this figure are in layer IV of area 17 based upon the identification of the stripe of Gennari in the whole section (data not shown). A close-up view of the tip of a single electrode, labeled with an asterisk, is shown in Fig. 1B. We observed no local injury to this tissue, as indicated by the normal-appearing neurons near the electrode. A photograph of the implanted array is shown in Fig. 1C. In this dorsal view of the exposed

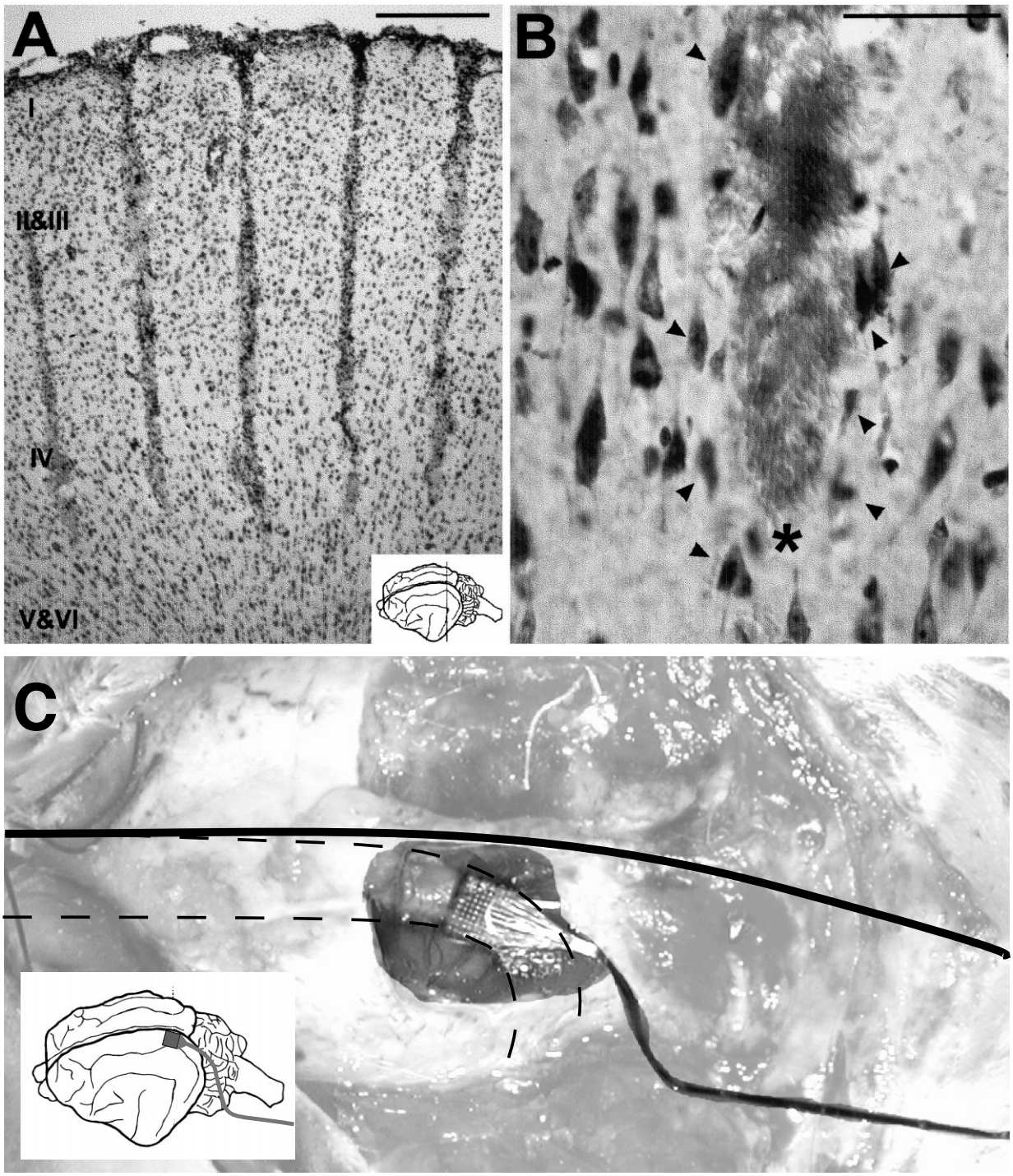

Fig. 1. Coronal transverse section through the left visual cortex (Nissl stain) and location of the array as implanted. (A) Low-power photomicrograph showing the position of the recording electrodes mainly in layer IV of area 17. Inset shows the position and orientation of the section. (B) Close-up view of one of the electrode tracks (asterisk). Notice the normal-appearing neurons (arrowheads) in close proximity to the electrode's active surface and the absence of local trauma. (C) Photograph of a dorsal view of the array after implanting in the cortex. In this figure, anterior is to the left and posterior to the right. To assist interpreting the photograph, the midline has been indicated with a solid line and the outline of the lateral and posterior lateral gyri has been indicated with a dashed line. Additionally, the contrast of the region outside the surgical opening has been reduced to emphasize the array location. The inset illustration shows the approximate location where the array was implanted relative to the entire cat brain. Scale bars = 400 μm (A); 50 μm (B).

cortex and array, the midline is shown as a solid line and the estimated outline of the lateral and the posterior lateral gyri are shown as dashed lines. For the animal shown here, the contralateral cortical hemisphere was also exposed to allow implantation of both hemispheres although a second array was not implanted at the time of the photograph. An illustration of the location of the array is provided in the inset to assist in interpreting the photograph. From sections such as shown in Fig. 1A, we concluded that the inner seven or eight rows of the UEA were in layer IV or at its borders in the animal studied.

RESULTS

General observations about receptive field characteristics

Figure 2 illustrates a three-dimensional projection of the four-dimensional receptive field data for three units that were measured simultaneously. The data for each unit represent the maximal response across one dimension, the latency between the visual stimulus and the occurrence of a spike. The three peaks represent the location and response magnitude of the receptive field for each of the three units. Below these peaks, the same data are represented as contour lines. The outermost contour line, at a magnitude of 4.3 standard deviations (the threshold for significance, see Experimental Procedures), shows the boundary of the excitatory receptive field. The rightmost peak and the center peak come from two units simultaneously measured on a single electrode, whereas the leftmost peak was recorded from an electrode 3.4 mm away.

The three units illustrated in Fig. 2 were selected specifically to show three non-overlapping receptive fields. More typically, the receptive fields recorded either on the same electrode or with different electrodes overlapped. Figure 3 shows 12 simultaneously measured receptive

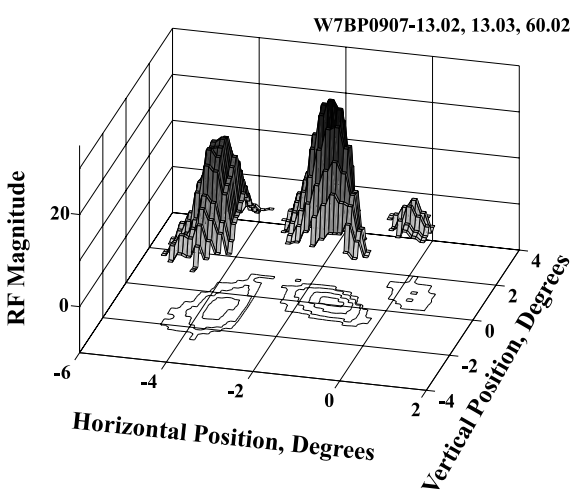

Fig. 2. Receptive field data for three units measured in parallel. The three peaks represent the statistic, measured in numbers of standard deviations, calculated by the reverse correlation method. The three sets of contour lines represent the same data collapsed into a two-dimensional representation. The outermost contour line for each set is the boundary of the receptive field. The small peak and the center peak come from two units isolated on a single electrode. The third peak is from an electrode 3.4 mm away.

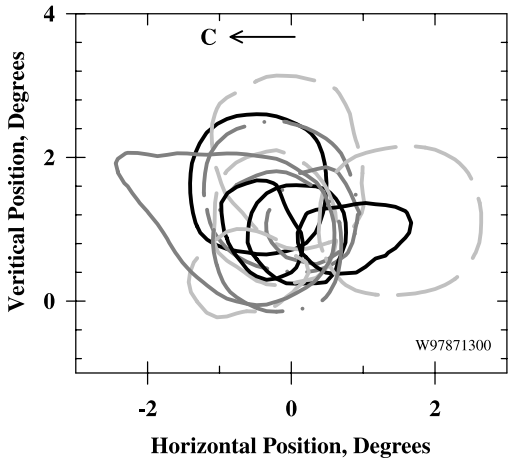

Fig. 3. Boundaries of 12 simultaneously measured receptive fields found in a single measurement of the receptive field properties. The arrow labeled with the letter C indicates the direction of the contralateral visual field for the particular experiment. In this example, representative of all the results for all measurements in all animals, the receptive fields are located near the visual representation of area centralis and have a tendency to be in the contralateral visual field.

field boundaries from a single 30-min period of data acquisition for one eye of one animal. Although it is difficult to distinguish individual receptive field boundaries, the figure clearly shows substantial overlap in the receptive fields. For example, some regions in visual space are contained in eight of the 12 receptive fields. Despite the difficulty in differentiating individual boundaries in the figure, these data represent one of the easiest to differentiate cases. In other experiments where larger numbers of receptive fields were recorded, the individual receptive field boundaries are more difficult to distinguish and regions of visual space are represented in even greater numbers of receptive fields.

All of the receptive field boundaries shown in Fig. 3 were within 4° of the visual representation of area centralis and the majority of the receptive fields were in the visual field contralateral to the hemisphere implanted. The locations of the receptive field boundaries in this figure were representative of the boundaries observed across all animals and eyes. Across all the measurements, the receptive fields were within 8° of the visual representation of area centralis. Further, they either straddled the vertical meridian or were located entirely in the contralateral visual field. This was expected since the UEA was implanted on the dorsal surface of the cortex at the junction of the lateral and posterior lateral gyri. For this region of the primary visual cortex, receptive fields should be located in the proximity of the visual representation of area centralis. Further, they generally should be located in the contralateral visual field (Tusa et al., 1978). On average, the majority of the receptive field boundaries were contained within a 4° horizontal by 5° vertical region of visual space, with its absolute location in visual space varying between animals.

The receptive field size and its trend with eccentricity were also consistent with that reported elsewhere. Figure

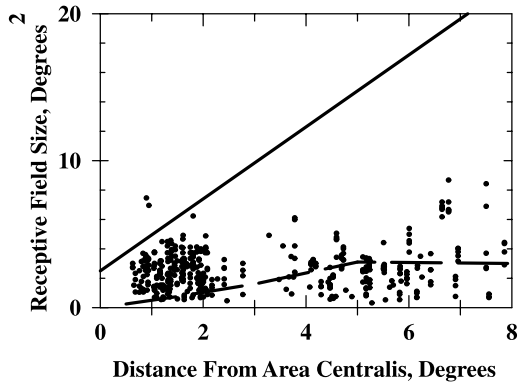

Fig. 4. Receptive field size as a function of eccentricity. The upper solid line is the upper limit and the dashed line is the average observed by Albus (1975b). With few exceptions, all receptive field sizes were within this upper limit. The average receptive field size was 2.7 ± 1.5 degrees^2, equivalent to a width of $1.6 \pm 0.44°$.

4 shows the receptive field size as a function of the distance of its center from the visual representation of area centralis. In the figure, the upper bound of receptive field size of simple cells reported by Albus is displayed as a solid line and the mean reported by Albus as a dashed line (Albus, 1975b). With two exceptions, all of the receptive field sizes were within the upper bound. For small eccentricities, our data show a tendency for the average receptive field size to be larger than that found by Albus, likely the result of two potential sources of error in our data. First, the large size of each square of the checkerboard, between 1 and 1.2 degrees^2, tends to limit the lower range of the size estimation. Second, the method used to establish the location of area centralis can result in a few degrees of error in the eccentricity. Hence, the larger than expected sizes observed at a small eccentricity may actually have larger eccentricities. No meaningful difference in the size measurement was observed between repeated measurements within the same animal and eye, indicating that the size can be measured reliably (multi-way ANOVA with repeated measures, $\alpha = 0.025$). On the other hand, there is statistical evidence to conclude that the average size was larger in animals with receptive fields further from area centralis (multi-way ANOVA with repeated measures, $P < 0.001$). Despite the trend for increasing size with eccentricity, most authors report a single, average size for all parafoveal receptive fields. Following suit, the average monocular receptive field size for all cats was 2.7 ± 1.5 degrees^2; a good match to the size of 2.8 degrees^2 reported for layer IV simple cells (Leventhal and Hirsch, 1978). Assuming a square receptive field, the average width was $1.6 \pm 0.44°$.

Local visuotopic map

To analyze the visuotopic organization of receptive fields, we collapsed the three-dimensional representation of each receptive field into a two-dimensional point in visual space by calculating the center of mass of the region contained within its boundary. We then applied a least-mean-squared-error fit to a linear transformation from the electrode loci to their representation in visual space.

Figure 5 illustrates the results of one such fit. The rectangle of small, open circles represents the outline of the UEA as mapped into visual space with each symbol indicating the location of an electrode along the periphery of the UEA. The large filled circle and filled square represent the electrode sites at the most rostral-lateral and rostral-medial corners of the UEA, respectively. The visual space representations of electrode sites having reliable receptive fields are represented by crosses. Each of these crosses is connected to an open square that represents the location in visual space of the center of mass of the receptive field mapped at the electrode site. The least-mean-squared-error fit minimizes the root-sum-squared length of these lines. The inset figure displays a two-dimensional scatter diagram of the error in the fit. This is equivalent to plotting the location of the receptive fields after translating each electrode locus to the origin. Additionally, the inset figure shows the 99% and 99.9999% probability contours of the measurement error as two concentric circles about the origin (see Appendix).

Because the locations of the receptive fields and the transformed electrode sites do not superimpose, the map from cortical space (the UEA) to visual space (receptive field locations) is clearly not linear. Furthermore, the map is not conformal as can be seen by inspection. Since some measurement error is expected, we would not anticipate perfect overlap but instead would expect to observe a small scatter in the receptive field locations around the transformed positions of the electrodes. Empirically, one can see that this is not the case by examining the scatter diagram inset of Fig. 5. Of the 25 receptive fields displayed, 80% have receptive fields that are located outside the 99.9999% probability of occurrence of measurement error. Statistical evidence supports the conclusion that the distribution of the observed radii of the residue vectors is not a result of measurement error (Kolmogorov–Smirnov test, $P < 0.001$). As the receptive fields were recorded simultaneously, the scatter is not a result of eye drift. Further, the scatter is not due to the method of selecting the receptive field center. Alternative methods of deriving the center, such as the centroid of the receptive field or the location of the peak in the receptive field, result in a similar degree of scatter. The most plausible explanation is that the map is neither linear nor conformal. The lack of linearity or conformality was observed across all measurements in all animals.

A closer examination of Fig. 5 indicates the degree of the non-linearity of the visuotopic projection. In some instances, one example being the electrode site labeled a, the receptive field center nearly overlies the electrode position. There are other cases, two examples being the electrode sites labeled b and c, where the receptive field center was separated from the electrode position by a number of degrees. Toward the center of the array were two receptive fields with similar locations, yet the electrodes associated with these receptive fields, labeled d and e, were separated by almost 1.8 mm. At the electrode

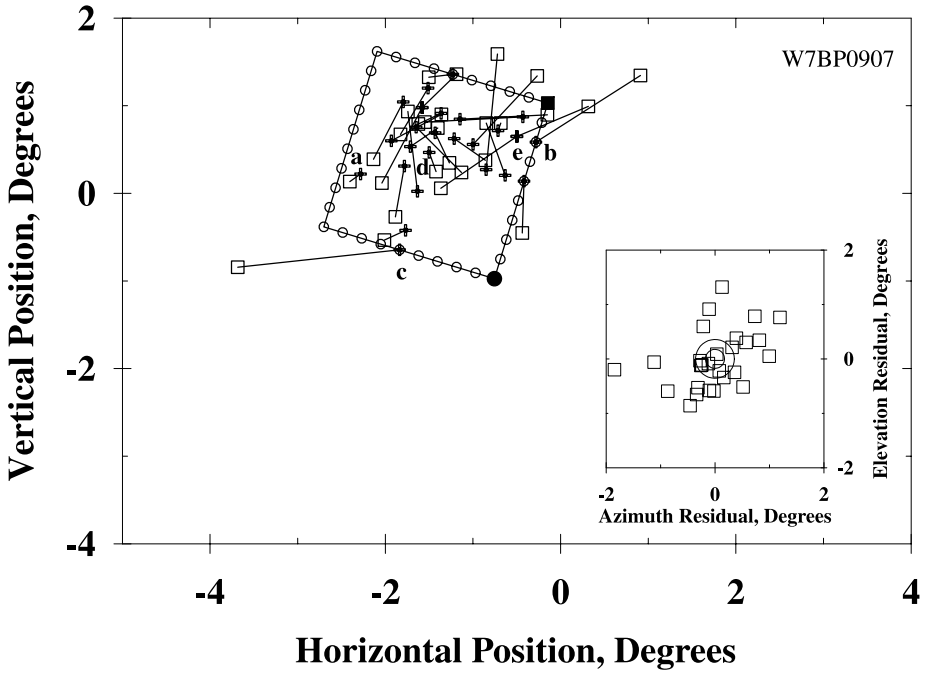

Fig. 5. Visual space representation of the electrode array resulting from a least-mean-squared-error fit of the electrode loci to their associated receptive field positions. The small open circles signify the electrode loci along the periphery of the electrode array. The larger filled circle and filled square indicate the rostral-lateral and rostral-medial corners of the array, respectively. Each cross and unfilled square connected by a line represent the position of an electrode and its associated receptive field, respectively. The inset figure presents the residuals as unfilled squares. The concentric lines represent two isoprobability levels of the measurement error, 99% and 99.9999%. The scatter in residues cannot be explained as a result of measurement error, indicating the map is not linear. By inspection, the map is not conformal.

labeled e, two units were found on the same electrode, yet their receptive fields locations were separated by almost 2°.

Although individual receptive fields do not follow a linear or conformal map, one does see the global organization described elsewhere (Tusa et al., 1978) when examining the average organization described by the fit across a large number of receptive fields. This can be seen by examining the outline of the array as mapped into visual space. As one progresses from the caudal to the rostral side of the array, the receptive field locations are generally at lower elevations. Similarly, as one progresses from the lateral to the medial edge of the array, the locations generally are located further into the contralateral visual field from the vertical meridian. In general, the average organization observed in all animals followed the organization given by Tusa et al. (1978). It should be noted that the orientation of the array typically was not aligned with the rostral to caudal and medial to lateral axes. Instead, it was placed based upon the available space from the craniotomy and cortical vasculature. Typically, it was oriented within 20° of the principal axes of the animal.

Repeated measurements of the receptive field positions were made within an animal over a 5–10-h period, and the average organization such as that shown by the array outline in Fig. 5 could be reproduced very reliably. Figure 6 shows the outline of the array mapped onto visual space for each measurement of the receptive field organization for three of the four animals. The upper two sets of outlines, labeled A and B, came from the positions measured with the contralateral and the ipsilateral eyes in the same animal, respectively. The lower two sets of outlines, labeled C and D, came from the positions measured with the contralateral eye in two other animals. In the case labeled D, the symbols indicating the location of electrodes on the periphery of the array are not illustrated to ease comparison of the outlines for this animal. In most cases, the outlines have similar orientations and positions within an animal. The small shifts in orientation and position observed are likely the result of not using identical units for all fits within an animal. Recalling that a reliable unit is one that generated a receptive field in at least three measurements, it is possible to use a different set of units in each of the fits within an animal. This effect is the source of the single thin outline seen in the group of outlines labeled B. A change in the position or orientation of the array outline without a concurrent change in the size suggests that eye drift occurred between the measurements. While this is not apparent for the three animals represented in Fig. 6, significant eye drift did appear to have happened in a fourth animal (data not shown).

There is statistical support for the empirical conclusion that there is no meaningful difference in the size of the outline between the repeated fits of the array to visual space. An analysis of the length of the residue vector within an animal indicates that there is no meaningful difference between repeated measurements of the receptive field properties (multi-way ANOVA with repeated measurements, $\alpha = 0.025$). As this analysis examines the residue vectors, changes in the absolute position in visual

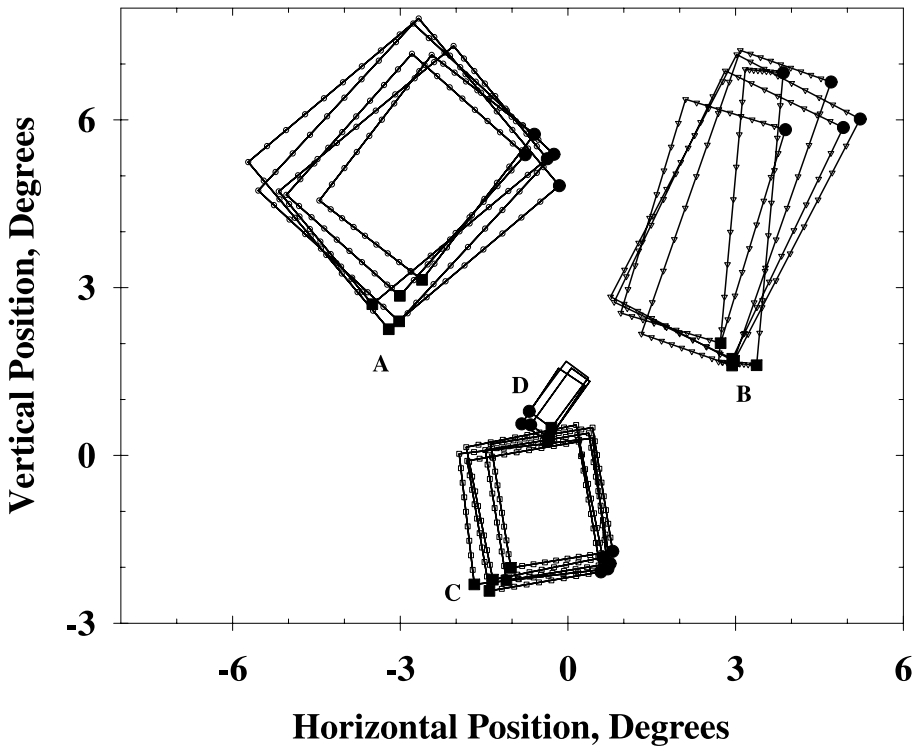

Fig. 6. Visual space representation of the outline of the electrode array for a series of measurements of the receptive field properties in three animals. The upper two sets of outlines, labeled with the letters A and B, come from measurements in the contralateral and ipsilateral eyes in the same animal, respectively. The other two sets of outlines, labeled C and D, come from measurements in the contralateral eye in two other animals. The smaller unfilled symbols indicate the locations of the electrode loci on the periphery of the array. These symbols were not drawn for the set of outlines labeled D for figure clarity. The larger filled square and filled circle are drawn at the electrode sites representing the most rostral-medial and rostral-lateral corners of the array, respectively. These data demonstrate the stability of the cortical to visual space mapping technique.

space of the array, the result of eye drift, do not affect the result. On the other hand, there is statistical evidence to conclude that the length of the residues differed between animals ($P < 0.001$, multi-way ANOVA with repeated measurements). The single animal where the UEA overlays area centralis appears to have significantly smaller residues in comparison to the other three animals. When this animal is removed from the analysis, no significant difference is seen between animals.

Magnification factor

The length of the side of the array outline when mapped into visual space gives an indication of the linear magnification factor from cortical space to visual space. The magnification factor has been quantified both as an areal magnification, having units of mm^2 of cortex per $degree^2$ of visual space (Tusa et al., 1978), and as a linear magnification, having units of mm of cortex per degree of visual space (Albus, 1975b). Table 1 summarizes the average magnification factor, in both forms, for our data in each animal. Due to the nature of the fit from cortical space to visual space, our approach averages the magnification factor along the side of the array. This approach is similar to that used by Tusa et al., who calculated the magnification factor after mapping the average receptive

Table 1. Magnification factor for each animal presented as a mean ± S.D.

Animal	Eye	Eccentricity (°)		Areal	Linear	
		Horizontal	Vertical		Rostral–caudal	Medial–lateral
1	Contralateral	−1.6	0.1	2.56 ± 0.43	1.82 ± 0.10	1.41 ± 0.25
	Ipsilateral	1.0	−0.7	7.30 ± 2.38	4.21 ± 2.80	2.21 ± 1.16
2	Contralateral (A)	−2.8	5.1	1.22 ± 0.32	1.24 ± 0.23	0.97 ± 0.09
	Ipsilateral (B)	2.9	4.3	1.80 ± 0.93	2.45 ± 1.43	0.76 ± 0.08
3	Contralateral (C)	−0.50	−0.92	2.75 ± 0.28	1.54 ± 0.04	1.79 ± 0.16
4	Contralateral (D)	−0.19	0.98	22.8 ± 2.53	3.05 ± 0.15	7.52 ± 0.98

The magnification factor is presented both as an areal magnification (mm^2 of cortex per $degree^2$ of visual space) for comparison to Tusa et al. (1978) and as a linear magnification (mm of cortex per degree of visual space) for comparison to Albus (1975b). Our results are similar to those found by both these authors. The letter shown after the type of eye (ipsilateral or contralateral) corresponds to the set of outlines in Fig. 6.

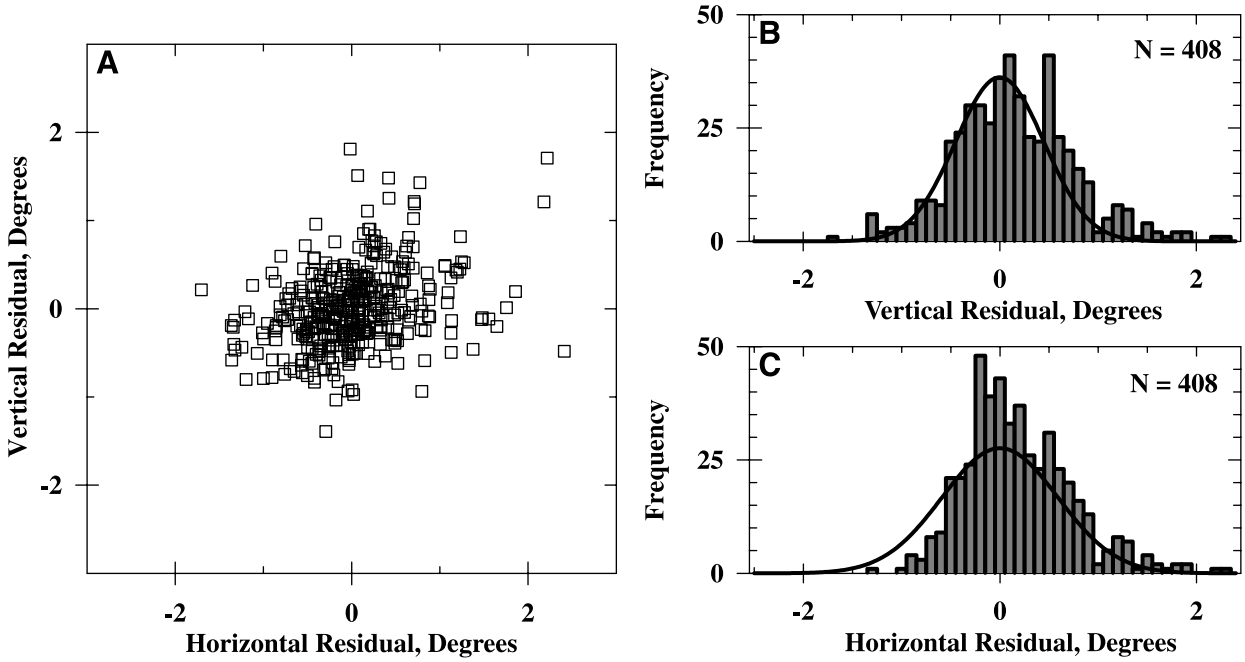

Fig. 7. Distribution of residuals resulting from least-mean-squared-error fit of electrode loci to associated receptive field position. (A) Residuals presented as two-dimensional scatter diagram. (B) Residual in the vertical axis. (C) Residual in the horizontal axis.

field location onto the electrode position. In contrast, Albus calculated the magnification factor as the average of the magnification factors between pairs of cells. Our data are consistent with those of both Tusa et al. and Albus.

Both Albus and Tusa et al. have shown that the magnification factor decreases with eccentricity with a steep slope within the first 10° from area centralis. We also observe this effect. The clearest indication of this is seen in Fig. 6. The transformed electrode array outlines located further from area centralis are larger, indicating a smaller magnification factor. Although the change in magnification factor with eccentricity appears striking in the two sets of outlines labeled C and D in Fig. 6, the large difference for what appear to be similar eccentricities is likely an artifact of the imprecision in calculating the eccentricity. As the location of area centralis can only be estimated to within a few degrees when using retinal landmarks (Nikara et al., 1968), the case labeled C could be further from area centralis. A statistical analysis of the areal magnification factor indicates that there is no meaningful difference between repeated measurements within an animal (multi-way ANOVA with repeated measurements, $\alpha = 0.025$). On the other hand, there is statistical evidence that the factor differed between animals for the same eye (multi-way ANOVA with repeated measurements, $P < 0.001$).

Receptive field scatter

The difference between the predicted location of a receptive field, assuming a linear visuotopic map, and the actual location measured has been termed the receptive field scatter (Hubel and Wiesel, 1974). In terms of our data, the scatter for a single unit is the residue vector for that unit after fitting the array to visual space. A compilation of the residue data is shown in Fig. 7A. These residuals are similar to those presented in the inset of Fig. 5 but contain data across all measurements in three of the four animals studied here. The residuals were significantly smaller in the animal where the transformed outline of the UEA overlay area centralis and these data are not shown in Fig. 7 nor were they used in calculating the statistics. Histograms of the vertical and horizontal axis residues are shown in Fig. 7B,C, respectively. Overlying each of these histograms is the normal probability distribution that best describes the data. The standard deviations of the horizontal and vertical axis residues are 0.59° and 0.45°, respectively. As the residues come from a least-mean-squared-error fit, the means tend to zero. There is statistical evidence supporting the conclusion that the two standard deviations differ (two-tailed variance ratio test, $P < 0.001$). This is simply an indication that the scatter in the horizontal direction is greater than that in the vertical direction. Additionally, the two residues are correlated (Kendall's τ, $P < 0.001$). Although not clear from Fig. 7A, the two residues tend to share the same sign. There is no evidence to conclude that either the horizontal or vertical axis residues are not normally distributed (Kolmogorov–Smirnov test, $\alpha = 0.025$). As a result, the residue can be modeled as a bivariate normal distribution with zero means, standard deviations of 0.59° and 0.45° in the horizontal and vertical axes, respectively, and correlation coefficient 0.32.

As the transformation from cortical space to visual space is fit to a linear map, one can readily invert the transformation to find the map from visual space to cortical space. Consequently, the residues can be presented as a cortical distance. Here, the residue describes the

difference in the cortical distance between the location of the electrode and the location one would predict the electrode to be given the receptive field position in visual space. In this coordinate frame, the residue is modeled as a bivariate normal distribution with zero mean, standard deviations of 1.5 mm in both the medial to lateral and the rostral to caudal directions, and a correlation coefficient of 0.23.

DISCUSSION

Our results compare well with and further extend the findings of other investigators. The average monocular receptive field size for all cats, the majority of which were in layer IV based on our histological findings, was 2.7 ± 1.5 degrees^2. This is in close agreement with the receptive field size of 2.8 degrees^2 reported by Leventhal and Hirsch (1978) for layer IV simple cells but larger than the median receptive field size of 1.8 degrees^2 reported by Gilbert (1977) for layer IV simple cells and the approximately 2 degrees^2 reported by Hubel and Wiesel (1962) for simple cells of all laminae. Assuming a square receptive field, the average width was $1.6 \pm 0.44°$. The similarity of receptive field size, despite the clear methodological differences between the referenced studies, which all used a hand mapping technique, and our statistically driven, reverse correlation technique, give credence to our statistical argument for the receptive field boundary. The majority of the units (57%) were driven exclusively by visual stimulation of the contralateral eye. Other investigators also have reported a predominance of contralateral input to the central region of primary visual cortex in the cat (Hubel and Wiesel, 1962; Albus, 1975a). Further, only a small portion of the units were binocularly driven (24%), a finding in agreement with other researchers (Gilbert, 1977; Leventhal and Hirsch, 1978).

Visuotopic mapping

In the global sense, our results generally concur with the visuotopic maps described by Hubel and Wiesel (1962) and Tusa et al. (1978). That is, units located more medially and caudally on the array tend to have receptive fields located in more contralateral and superior regions of visual space, respectively. However, when examining pairs or small groups of closely spaced electrodes, we have observed a large degree of non-conformality in the translation from visual space to cortical space. As a consequence, even if one knows the average visuotopic organization of the central region of cat primary visual cortex, the error in estimating the location of the receptive field position for a particular neuron in the region is distributed with zero mean and has a standard deviation of 0.59° and 0.45° in the horizontal and vertical directions, respectively. This scatter in the receptive field position is clearly not due to either measurement error, being almost an order of magnitude greater than the estimated error, or eye drift, as the recordings were made simultaneously for all active electrodes.

Scatter also has been expressed as a cortical distance. This has been done principally in terms of the electrode separation that assures non-overlapping receptive fields (Hubel and Wiesel, 1974; Albus, 1975b). In terms of a cortical distance, the scatter we observed is distributed with zero means and has a standard deviation of 1.5 mm in each of the medial to lateral and the rostral to caudal directions. Here the scatter describes the distribution of the difference between the actual recording site and the predicted electrode site, the latter estimated from the receptive field location. From this probabilistic description of the scatter, the metric described above can be calculated readily. In order to address the electrode separation to assure non-overlapping receptive fields, we converted the average monocular receptive field width into a cortical distance by multiplying by the horizontal and vertical cortical magnification factors. We found that one must traverse 2.0 mm tangentially in cortex before having an 80% probability of observing non-overlapping monocular receptive fields. This value is similar to values reported by other investigators. Hubel and Wiesel (1974) reported that one must traverse 1–2 mm of monkey primary visual cortex to observe non-overlapping receptive fields. In cat primary visual cortex, Albus (1975b) reported that one must traverse 2.4 mm before observing non-overlapping receptive fields. These results do not imply that electrodes separated by smaller distances necessarily have overlapping receptive fields. Given the distributions of the scatter and receptive field size, it is possible to have non-overlapping receptive fields on two closely spaced electrodes. An example of this was shown in Fig. 2, where two non-overlapping receptive fields were observed for two units isolated from recordings made with a single electrode.

Tiling necessary to assure adequate coverage

From the distributions of the receptive field scatter and size, one can develop a distribution that describes the probability that a location in visual space is within a receptive field, given the expected site of the receptive field center. After performing a simple Monte Carlo simulation, we empirically found that this distribution is well described by a normal distribution centered at the expected receptive field center and having 0.82° standard deviation. The coverage afforded by the entire array can then be calculated as the sum of a series of these distributions, each of which is centered at the regularly spaced grid of the array, after being translated into visual space. By this mechanism, one can investigate the changes in coverage resulting from a change in electrode spacing. In this analysis, we assumed only a 25% probability of recording data at any given electrode site, the average observed in this study. Further, we assumed a magnification factor of 1.5 mm of cortex per degree of visual space, the average across our measurements. For the present 0.4-mm electrode spacing of a 100-electrode array, we found that regions of visual space representing the center of the array will likely be contained in three receptive fields. At an electrode spacing of 0.75 mm, the

likelihood drops to the region being in only one receptive field.

Implications for a vision neuroprosthesis

The results of this mapping study have implications in the field of neuroprosthetics. The UEA was initially developed as an intracortical stimulation device under the hypothesis that patterned electrical stimulation would evoke patterned perceptions. Our results indicate that the mapping of receptive fields with respect to the electrode grid is locally non-conformal when examined with our present 0.4-mm interelectrode spacing. That is, although one can predict the average location of a receptive field sensed at a single electrode based upon an average visuotopic map, the actual location might be widely distributed about the average point. It is not until one moves to larger interelectrode spacing that one begins to observe the roughly conformal visuotopic organization reported elsewhere (Albus, 1975b; Tusa et al., 1978).

The vision prosthesis work of Brindley and coworkers indicates that there is also randomness in the location of phosphenes evoked in primary visual cortex in man. They reported "Non-adjacent electrodes can give phosphenes that are very near to each other in the visual field, and adjacent electrodes can give phosphenes that are not near to each other" (Brindley and Lewin, 1968). More recently, it has been reported that stimulation with intracortical microelectrodes separated by less than 0.5 mm may produce fused phosphenes (Bak et al., 1990; Schmidt et al., 1996). Consequently, larger interelectrode spacing may be necessary to produce distinct phosphenes – a conclusion supported by our feline physiological experiments. Our results, in concert with the results of other researchers, recommend an electrode spacing of 0.5–1.2 mm for a neuroprosthetic application. The optimal spacing awaits further psychophysical experiments in humans to investigate whether discrete or partially overlapping phosphenes provide a more useful visual sense.

Under the presumption that the perceptual phosphene organization evoked by electrical stimulation follows the visuotopic organization, one can use the tiling analysis methodology described above to investigate the electrode spacing necessary to fully tile visual space for a visual neuroprosthesis. At this point, one can only speculate, as the magnification factor and degree of scatter are poorly quantified in humans. Hence, a number of assumptions must be made apart from the admittedly poor choice of the cat as a model of human visual cortex. First, we assumed a similar magnitude of magnification and scatter as we observed in the cat, an assumption supported by similarities in our results to those observed in primates (Hubel and Wiesel, 1974). Next, we assumed a 0.9° phosphene diameter, the middle of the range of sizes reported by Schmidt et al. (1996). Finally, we assumed a 66% probability of evoking a phosphene, the probability of evoking a behavioral response by electrical stimulation of primary auditory cortex in the cat with the UEA (Rousche and Normann, 1999). Under these assumptions, an electrode spacing of 1.2 mm or less will give near unity probability of filling visual space. At this spacing, a 25×25 grid of electrodes will fill a $19\times19°$ field, roughly the size of the display on a 13-inch monitor at arm length. Clearly, the size of such an array of electrodes, 3×3 cm, prohibits the use of a single, rigid structure. Instead, multiple, smaller arrays may be used or a single array with a compliant base. Even with such architectures, the curvature of the gyri would generally not allow access to cortex deep within sulci. At the present 0.4-mm interelectrode spacing, the UEA is expected to provide redundancy in phosphene representation. One can take advantage of this redundancy by interleaving stimulation at each of the sites, thereby opening the possibility of mitigating the potential deleterious effects of chronic electrical stimulation of cortex: tissue damage, cortical reorganization, and kindling. The design of a vision prosthetic system will have to be flexible enough to accommodate the non-conformality in the visuotopic mapping as well as manage redundancy in evoked phosphenes.

Acknowledgements—The authors thank Yanping Zhang for fabricating the arrays used in this study and Ido Perlman, Ph.D. for reviewing the manuscript. This work was performed under the State of Utah Center of Excellence Program and NSF Grant IBN 94-24509.

REFERENCES

Albus, K., 1975a. Predominance of monocularly driven cells in the projection area of the central visual field in cat's striate cortex. Brain Res. 89, 341–347.

Albus, K., 1975b. A quantitative study of the projection area of the central and the paracentral visual field in area 17 of the cat. I. The precision of the topography. Exp. Brain Res. 24, 159–179.

Bak, M., Girvin, J.P., Hambrecht, F.T., Kufta, C.V., Loeb, G.E., Schmidt, E.M., 1990. Visual sensations produced by intracortical microstimulation of the human occipital cortex. Med. Biol. Eng. Comput. 28, 257–259.

Bishop, P., Kozak, W., Vakkur, G., 1962. Some quantitative aspects of the cat's eye: Axis and plane of reference, visual field co-ordinates and optics. J. Physiol. 163, 466–502.

Brindley, G.S., Lewin, W.S., 1968. The visual sensations produced by electrical stimulation of the medial occipital cortex. J. Physiol. 194, 54–55P.

Cicerone, C.M., Green, D.G., 1977. Control of eye movements while recording from single units in the pigmented rat. Vis. Res. 17, 985–987.

DeAngelis, G.C., Ghose, G.M., Ohzawa, I., Freeman, R.D., 1999. Functional micro-organization of primary visual cortex: receptive field analysis of nearby neurons. J. Neurosci. 19, 4046–4064.

Dow, B.M., Vautin, R.G., Bauer, R., 1985. The mapping of visual space onto foveal striate cortex in the macaque monkey. J. Neurosci. 5, 890–902.

Eckhorn, R., Krause, F., Nelson, J.I., 1993. The RF-cinematogram. A cross-correlation technique for mapping several visual receptive fields at once. Biol. Cybern. 69, 37–55.

Gilbert, C.D., 1977. Laminar differences in receptive field properties of cells in cat primary visual cortex. J. Physiol. 268, 391–421.
Guillory, K.S., Normann, R.A., 1999. A 100-channel system for real time detection and storage of extracellular spike waveforms. J. Neurosci. Methods 91, 21–29.
Hetherington, P.A., Swindale, N.V., 1999. Receptive field and orientation scatter studied by tetrode recordings in cat area 17. Vis. Neurosci. 16, 637–652.
Hubel, D.H., Wiesel, T.N., 1962. Receptive fields, binocular interaction and functional architecture in the cat's visual cortex. J. Physiol. 160, 106–154.
Hubel, D.H., Wiesel, T.N., 1974. Uniformity of monkey striate cortex: a parallel relationship between field size, scatter, and magnification factor. J. Comp. Neurol. 158, 295–305.
Jain, A.K., Duin, R.P.W., Mao, J., 2000. Statistical pattern recognition: A review. IEEE Trans. Pattern Anal. Mach. Intell. 22, 4–37.
Jones, J.P., Palmer, L.A., 1987. The two-dimensional spatial structure of simple receptive fields in cat striate cortex. J. Neurophysiol. 58, 1187–1211.
Jones, K.E., Campbell, P.K., Normann, R.A., 1992. A glass/silicon composite intracortical electrode array. Ann. Biomed. Eng. 20, 423–437.
Leventhal, A.G., Hirsch, H.V., 1978. Receptive-field properties of neurons in different laminae of visual cortex of the cat. J. Neurophysiol. 41, 948–962.
Lewicki, M.S., 1998. A review of methods for spike sorting: the detection and classification of neural action potentials. Network 9, R53–78.
Nikara, T., Bishop, P.O., Pettigrew, J.D., 1968. Analysis of retinal correspondence by studying receptive fields of binocular single units in cat striate cortex. Exp. Brain Res. 6, 353–372.
Nordhausen, C.T., Maynard, E.M., Normann, R.A., 1996. Single unit recording capabilities of a 100 microelectrode array. Brain Res. 726, 129–140.
Rodieck, R.W., Pettigrew, J.D., Bishop, P.O., Nikara, T., 1967. Residual eye movements in receptive-field studies of paralyzed cats. Vis. Res. 7, 107–110.
Rousche, P.J., Normann, R.A., 1992. A method for pneumatically inserting an array of penetrating electrodes into cortical tissue. Ann. Biomed. Eng. 20, 413–422.
Rousche, P.J., Normann, R.A., 1999. Chronic intracortical microstimulation (ICMS) of cat sensory cortex using the Utah Intracortical Electrode Array. IEEE Trans. Rehabil. Eng. 7, 56–68.
Sahani, M., Pezaris, J.S., Andersen, R.A., 1997. On the separation of signals from neighboring cells in tetrode recordings. In: Advances in Neural Information Processing Systems 11, Denver, CO.
Schmidt, E.M., Bak, M.J., Hambrecht, F.T., Kufta, C.V., O'Rourke, D.K., Vallabhanath, P., 1996. Feasibility of a visual prosthesis for the blind based on intracortical microstimulation of the visual cortex. Brain 119, 507–522.
Tootell, R.B., Silverman, M.S., Switkes, E., De Valois, R.L., 1982. Deoxyglucose analysis of retinotopic organization in primate striate cortex. Science 218, 902–904.
Tusa, R.J., Palmer, L.A., Rosenquist, A.C., 1978. The retinotopic organization of area 17 (striate cortex) in the cat. J. Comp. Neurol. 177, 213–235.

APPENDIX. PRECISION OF RECEPTIVE FIELD PROPERTY MEASUREMENTS

To quantify the precision with which we were able to measure receptive field properties, we compared the difference in receptive field position estimated with odd-numbered spikes to the estimate with even-numbered spikes. As both sets of spikes cover the entire test duration, they embody the same variability in responsiveness of the unit as well as change in eye position. The difference between the estimated positions should tend to zero with the magnitude of the difference indicating the precision of the estimate. Due to simultaneous recording of multiple units, we can make multiple comparisons within a period of data acquisition, all of which represent the same change in eye position as well as similar variability in the responsiveness. From the distribution of the difference in the estimated receptive field position, we are able to place a metric onto the variability of the measurement. The mean and standard deviation of these distributions are provided in Table 2. For all properties, there is no statistical evidence to conclude that average value in the difference is non-zero (two-tailed t-test comparing mean to zero, $\alpha = 0.025$). Of the properties, only the peak value exhibits statistical evidence to conclude it comes from a normal distribution (Kolmogorov–Smirnov test, $\alpha = 0.025$). The other distributions are leptokurtic.

Of these data sets, the distribution of the difference in receptive field position is the most germane to our results. The difference between the standard deviations in the horizontal axis (0.080°) and the vertical axis (0.070°) is insignificant for the sample size (two-tailed variance ratio test, $\alpha = 0.025$), and a pooled variance of 0.075° can be assumed. The distributions of the error in measurement in the horizontal and vertical axes are similarly distributed (Kolmogorov–Smirnov test, $\alpha = 0.025$) and the errors are not correlated (Kendall's τ, $\alpha = 0.025$). Consequently, we can model the distribution of the measurement error as a circularly distributed function with zero mean and 0.075° standard deviation.

To discern whether there was a systematic effect within our measurements, we compared the receptive field positions estimated with spikes from the first half of a period of data acquisition to that estimated by spikes from the second half of the period. As a systematic effect would equally affect all receptive field positions within each half of the period of data acquisition, we collapsed the individual receptive field positions for each half period into a single, average position. We then analyzed the difference between the averages for the first and second half of the period of data acquisition. In most cases, the magnitude of the difference could be attributed to the measurement error. On the other hand, in two of the 18 periods of data acquisition, the magnitude of the difference exceeded a 99.9% probability of occurrence. In these cases, there was likely a systematic variation in the situation over the 15 min that separated the first and second halves of the period of data acquisition. This variation can result in up to a 0.4° shift in the measured position of the receptive field. The most plausible explanation of this shift is that, despite the administration of a paralytic agent, there was a change in eye position

Table 2. Statistics of the difference between the receptive field properties calculated with odd-numbered spikes and even-numbered spikes

Item	Mean	S.D.	Units
Change in peak value	0.126	0.952	
Change in area	0.024	0.233	Degrees^2
Change in horizontal position	−0.0045	0.0796	Degrees
Change in vertical position	0.0065	0.0698	Degrees

For all of the receptive field properties, there is no statistical evidence to conclude that the mean is not zero.

between the first and second halves of the test. This finding is similar to that observed by others (Rodieck et al., 1967; Cicerone and Green, 1977).

The precision of the estimation of receptive field size is the other measurement error of interest for this analysis. Unfortunately, the eye drift noted above confounds quantifying this precision. Were there significant eye drift during a test, one would anticipate the drift would result in an increase in the estimated size of the receptive field. Consequently, the estimate using either the odd- or the even-numbered spikes should be larger than the estimate using either the spikes from the first or second half of the test. A comparison of these four different size measurements showed no statistically significant difference (multi-way ANOVA with repeated measures, $\alpha = 0.025$), likely due to the large variability in the estimate. The precision of the size estimate was modeled as a normal distribution with zero mean and 0.23 degrees^2 standard deviation.

In summary, we have established the precision of our capability to estimate the receptive field position and size. The measurement error of the position is modeled as the joint distribution of two independent, normal distributions with zero means and 0.075° standard deviations. The measurement error of the size is modeled as a normal distribution with zero mean and 0.23 degrees^2 standard deviation. Further, we noted that there could be significant eye drift over an interval as brief as 15 min.

(*Accepted* 10 *April* 2001)